Singular Perturbation -Based Model Order Reduction and Accuracy Analysis of Matching Control Grid-Forming Converter

Feng Wu
NARI Group Corporation (State Grid Electric Power Research Institute)
Nanjing, China
wufeng@sgepri.sgcc.com.cn

Pan Feng
School of Electrical Engineering and Automation
Wuhan University
Wuhan, China
2023202070069@whu.edu.cn

Zhen Tian
School of Electrical Engineering and Automation
Wuhan University
Wuhan, China
ztian.ee@whu.edu.cn

Meng Huang
School of Electrical Engineering and Automation
Wuhan University
Wuhan, China
meng.huang@whu.edu.cn

Yushuang Liu
School of Electrical Engineering and Automation
Wuhan University
Wuhan, China
lyshuang@whu.edu.cn

Xiaoming Zha
School of Electrical Engineering and Automation
Wuhan University
Wuhan, China
xmzha@whu.edu.cn

Xiang Si
NARI Group Corporation (State Grid Electric Power Research Institute)
Nanjing, China
sixiang@sgepri.sgcc.com.cn

Xiancheng Ren
NARI Group Corporation (State Grid Electric Power Research Institute)
Nanjing, China
renxiancheng@sgepri.sgcc.com.cn

***Abstract*—With the growing penetration of renewable energy resources, the transient characteristics of the power system after large disturbance are increasingly affected by the multi-time-scale control loops of grid-connected converters. Establishing the mathematical model of grid-connected converter that takes into account both model accuracy and computational efficiency is important. In this paper, the full order and reduced order models of matching control grid-forming converter are developed based on singular perturbation theory, considering the impact of control loop interactions. By separating the state variables' reduced order component and model error component, the dynamic equations governing the model error components are derived. It is found that the model error component includes the impact of both control parameters and the reduced order components. Finally, the accuracy of the model error components is verified through simulation results. (*Abstract*)**

***Keywords—model order reduction, singular perturbation, grid-forming converter; control loop interactions.** (key words)*

I. Introduction

With the large-scale integration of renewable energy resources (REGs) into the power grid, the penetration of power electronic-based control equipment is growing. As a result, the transient stability characteristics of the power system after large disturbance is increasingly influenced by the coupling and interaction of multi-time-scale control loops of REGs. Therefore, developing the REG model that takes into account both model accuracy and computational efficiency is the basis for system simulation analysis and control decision-making.

This research receives funding from the Research on Key Technologies for Online Assessment of Ultra-Short-Term Safety Risks in New Power Systems of NARI Group's Science and Technology Project.

In terms of the model order reduction method, the singular perturbation theory (SPT) can separate the different time scale control dynamics, which can reduce the model order while preserving its mathematical structure[1].

Based on the SPT, extensive research have been conducted on the assessment of model accuracy. Reference [2] introduces a method based on singular perturbation parameters to assess model reduction accuracy, which gives the upper and lower boundary of the singular perturbation parameter. In [3], the accuracy of reduced order model is analyzed from the perspective of transient stability. The state space model of fast subsystem is established and its impact on system's transient stability is quantitatively analyzed. Literature [4] proposed a contraction theory-based model accuracy estimation method, which quantifies the convergence rate of fast dynamics and gives a criterion for parameter selection. Literature [5] established the energy function of different reduced order models derived from the singular perturbation theory. Then, based on the Takagi-Sugeno method, the attraction domain is employed as evaluation criterion to assess the accuracy of different reduced order models.

Based on the aforementioned research, there is still no unified framework for the selection of reduced-order models. In this paper, based on the SPT-based model order reduction, the reduced order model of matching control grid-forming converter is established. The state variables are decomposed into the reduced-order component and the model error component. A dynamic equation governing the model error component is accurately derived. Then, impact of parameters' variation on the model error component is analyzed. Finally, simulation results verify the accuracy of derived model error component and the parameters' impact, which can be employed as the criterion for the accuracy assessment of reduced order model.

979-8-3315-8138-1

II. System Description And Modeling

A. System Description

Figure 1 shows the main topology and controller structure of analyzed matching control grid-forming (GFM) converter connected to the power grid. The main circuit part includes the constant active power input P_{in}, DC capacitor C_{dc}, voltage source converter (VSC), filter inductor L_f and capacitor C_f, line inductor L_g and power grid. The converter's controller part includes matching control, reactive power control (RPC), frequency feedforward in RPC (FFIR) [6], virtual admittance control (VAC) and vector current control (VCC).

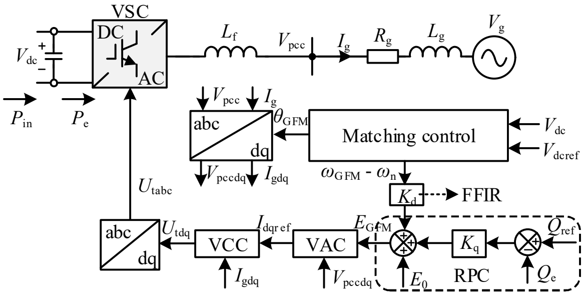

Fig. 1. Main topology and controller of the analyzed Matching control GFM-VSC.

B. Full Order Modeling of Matching control GFM-VSC

The matching control generates synchronization frequency based on the DC-link voltage control [1]:

$$K_{\text{pdc}}\left(V_{\text{dc}}-V_{\text{dcref}}\right)+\omega_{\text{n}}=\omega_{\text{GFM}} \tag{1}$$

The dynamic of DC-link bus capacitor is as follows:

$$P_{\text{in}}-P_{\text{e}}=C_{\text{dc}}V_{\text{dc}}\frac{dV_{\text{dc}}}{dt} \tag{2}$$

where P_e denotes the DC output active power of DC capacitor. There is $P_e = 1.5(V_{\text{pccd}}*I_{\text{gd}} + V_{\text{pccq}}*I_{\text{gq}})$.

VAC generates the reference value of dq-axis current:

$$\begin{cases} I_{\text{dref}}=\dfrac{E_{\text{GFM}}-V_{\text{pccd}}+\omega_{\text{n}}L_{\text{V}}I_{\text{qref}}}{sL_{\text{V}}+R_{\text{V}}} \\ I_{\text{qref}}=\dfrac{0-V_{\text{pccq}}-\omega_{\text{n}}L_{\text{V}}I_{\text{dref}}}{sL_{\text{V}}+R_{\text{V}}} \end{cases} \tag{3}$$

E_{GFM} is the internal voltage of VSC, which is regulated by both the RPC and FFIR:

$$E_{\text{GFM}}=K_{\text{q}}\left(Q_{\text{ref}}-Q_{\text{e}}\right)+K_{\text{d}}\left(\omega_{\text{GFM}}-\omega_{\text{n}}\right) \tag{4}$$

I_{gd} and I_{gq} are controlled by the VCC:

$$\begin{cases} \left(I_{\text{gdref}}-I_{\text{gd}}\right)\left(K_{\text{pc}}+\dfrac{K_{\text{ic}}}{s}\right)-\omega_{\text{n}}L_{\text{f}}I_{\text{gq}}+V_{\text{pccd}}=U_{\text{td}} \\ \left(I_{\text{gqref}}-I_{\text{gq}}\right)\left(K_{\text{pc}}+\dfrac{K_{\text{ic}}}{s}\right)+\omega_{\text{n}}L_{\text{f}}I_{\text{gd}}+V_{\text{pccq}}=U_{\text{tq}} \end{cases} \tag{5}$$

where K_{pc} and K_{ic} are the proportional gain and integral gain of VCC's PI controller. U_{td} and U_{tq} are the dq-axis components of the modulation voltage.

Except for the above controllers, the dynamic equation on the filter inductor L_f and line inductor L_g are as follows:

$$\begin{cases} V_{\text{pccd}}=V_{\text{g}}\cos\delta+\left(sL_{\text{g}}+R_{\text{g}}\right)I_{\text{gd}}-\omega_{\text{n}}L_{\text{g}}I_{\text{gq}} \\ V_{\text{pccq}}=-V_{\text{g}}\sin\delta+\left(sL_{\text{g}}+R_{\text{g}}\right)I_{\text{gq}}+\omega_{\text{n}}L_{\text{g}}I_{\text{gd}} \end{cases} \tag{6}$$

$$\begin{cases} U_{\text{td}}=V_{\text{pccd}}+sL_{\text{f}}I_{\text{gd}}-\omega_{\text{n}}L_{\text{f}}I_{\text{gq}} \\ U_{\text{tq}}=V_{\text{pccq}}+sL_{\text{f}}I_{\text{gq}}+\omega_{\text{n}}L_{\text{f}}I_{\text{gd}} \end{cases} \tag{7}$$

Combining (1) to (7), the full-order closed-loop nonlinear mathematical model is obtained, as seen in (8).

$$\begin{cases} d\omega_{\text{GFM}}/dt=K_{\text{pdc}}\,dV_{\text{dc}}/dt=K_{\text{pdc}}\left(P_{\text{in}}-P_{\text{e}}\right)/C_{\text{dc}}V_{\text{dc}} \\ d\delta/dt=\omega_{\text{GFM}}-\omega_{\text{g}}=K_{\text{pdc}}\left(V_{\text{dc}}-V_{\text{dcref}}\right)+\omega_{\text{n}}-\omega_{\text{g}} \\ L_{\text{V}}\dfrac{dI_{\text{dref}}}{dt}=E_{\text{GFM}}-V_{\text{pccd}}+\omega_{\text{n}}L_{\text{V}}I_{\text{qref}}-R_{\text{V}}I_{\text{dref}} \\ L_{\text{V}}\dfrac{dI_{\text{qref}}}{dt}=0-V_{\text{pccq}}-\omega_{\text{n}}L_{\text{V}}I_{\text{dref}}-R_{\text{V}}I_{\text{qref}} \\ L_{\text{f}}\dfrac{dI_{\text{gd}}}{dt}=\left(I_{\text{dref}}-I_{\text{gd}}\right)K_{\text{pc}}+x_{\text{gd}} \\ L_{\text{f}}\dfrac{dI_{\text{gq}}}{dt}=\left(I_{\text{qref}}-I_{\text{gq}}\right)K_{\text{pc}}+x_{\text{gq}} \\ \dfrac{1}{K_{\text{ic}}}\dfrac{dx_{\text{gd}}}{dt}=I_{\text{dref}}-I_{\text{gd}} \\ \dfrac{1}{K_{\text{ic}}}\dfrac{dx_{\text{gq}}}{dt}=I_{\text{qref}}-I_{\text{gq}} \end{cases} \tag{8}$$

The state variables include ω_{GFM}, δ, I_{dref}, I_{qref}, I_{gd}, I_{gq}, x_{gd} and x_{gq}. x_{gd} and x_{gq} are the output of VCC's integrator. The schematic diagram of the derived full-order nonlinear mathematical model is shown in Fig. 2. Considering the impact of matching control, dynamic of C_{dc}, VAC and VCC, the full order model is eighth-order.

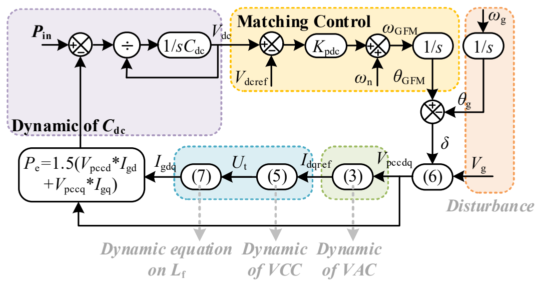

Fig. 2. Schematic diagram of the derived full-order closed-loop nonlinear mathematical model.

III. Model Order Reduction

The standard singular perturbation system is shown in (9):

$$\begin{cases} \varepsilon\dot{x}=f\left(x,y,\varepsilon\right) \\ \dot{y}=g\left(x,y,\varepsilon\right) \end{cases} \tag{9}$$

where x and y represent the relatively fast and slow state variable vectors, respectively. There is $x \in R_m$ and $y \in R_n$. m and n are the number of state variables of x and y. The parameter ε denotes the singular perturbation parameter, which determines the time scale separation of the state variables. The ε satisfies $0<\varepsilon \ll 1$.

The reduced order model (ROM) is derived by setting $\varepsilon = 0$ in (9), which reduces the system order from m+n to n. At the same time, the differential dynamics of x is eliminated, and an algebraic constraint equation is obtained. The resulting n-th order system, presented in (10).

$$\begin{cases} 0 = f(x, y, 0) \\ \dot{y} = g(x, y, 0) \end{cases} \tag{10}$$

For the derived eighth-order system (8), it is obvious that the system satisfies the standard form of SPT. Therefore, the high order differential dynamics of state variables I_{dref}, I_{qref}, I_{gd}, I_{gq}, x_{gd} and x_{gq} can be eliminated.

The fourth order model is shown in (11) and Fig. 3. In the fourth order ROM, the VCC is equivalent to a unit gain, which is also widely assumed [7].

$$\begin{cases} d\omega_{GFM}/dt = K_{pdc}\, dV_{dc}/dt = K_{pdc}(P_{in} - P_e)/C_{dc}V_{dc} \\ d\delta/dt = \omega_{GFM} - \omega_g = K_{pdc}(V_{dc} - V_{dcref}) + \omega_n - \omega_g \\ L_V \dfrac{dI_{dref}}{dt} = E_{GFM} - V_{pccd} + \omega_n L_V I_{qref} - R_V I_{dref} \\ L_V \dfrac{dI_{qref}}{dt} = 0 - V_{pccq} - \omega_n L_V I_{dref} - R_V I_{qref} \\ I_{dref} = I_{gd} \\ I_{qref} = I_{gq} \end{cases} \tag{11}$$

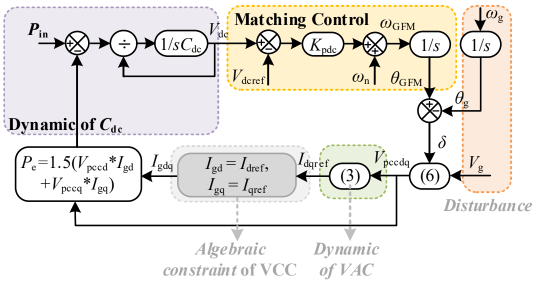

Fig. 3. Schematic diagram of the fourth-order ROM ignoring the differential dynamics of VCC.

The second-order model is shown in (12) and Fig. 4. In the second-order model, the current reference values are analytical algebraic equations with respect to δ and ω.

$$\begin{cases} d\omega_{GFM}/dt = K_{pdc}\, dV_{dc}/dt = K_{pdc}(P_{in} - P_e)/C_{dc}V_{dc} \\ d\delta/dt = \omega_{GFM} - \omega_g = K_{pdc}(V_{dc} - V_{dcref}) + \omega_n - \omega_g \\ I_{dref}(\delta, \omega) = \dfrac{R_V(E_{GFM} - V_g\cos\delta) + \omega_g L_V V_g \sin\delta}{(R_V)^2 + (\omega_n L_V)^2} \\ I_{qref}(\delta, \omega) = \dfrac{-\omega_g L_V(E_{GFM} - V_g\cos\delta) + R_V V_g \sin\delta}{(R_V)^2 + (\omega_n L_V)^2} \\ I_{gd} = I_{dref}(\delta, \omega) \\ I_{gq} = I_{qref}(\delta, \omega) \end{cases} \tag{12}$$

In order to compare the different response characteristics of different ROMs, the full-order model, fourth-order ROM and second-order ROM are constructed based on the MATLAB/ Simulink platform. System parameters are shown in table I.

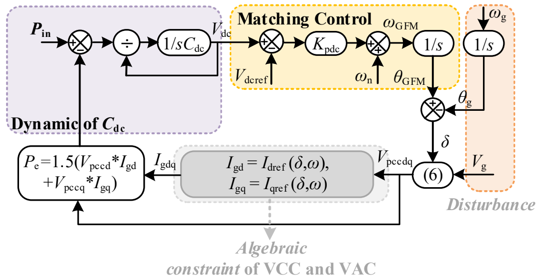

Fig. 4. Schematic diagram of the second-order ROM ignoring the differential dynamics of VCC and VAC.

TABLE I. PARAMETERS OF ANALYZED SYSTEM

Parameters	Value	Parameters	Value
P_{in}	30kW	K_d	2
C_{dc}	17mF	K_q	0.0001
L_f	0.5mH	Q_{ref}	0
L_g	4.5mH	V_{dcref}	750V
R_g	0.5Ω	K_{dc}	2
L_V	3mH	K_{pc}	2
R_V	0.5Ω	K_{ic}	20

Set the grid voltage amplitude dips to 0.6p.u. and recovers at 500ms. The transient active power waveforms under different ROMs are shown in Fig. 5. It is obvious that there are significant differences in active power responses among different models, especially within the short period after grid voltage dips and recovers.

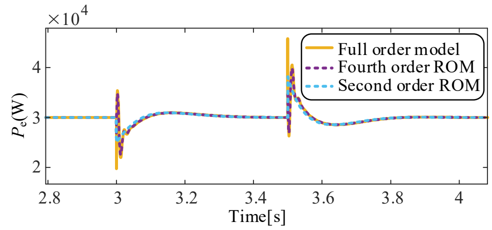

Fig. 5. Simulation waveforms under different models.

In addition, the simulation speed of different models are compared, including the electromechanical model, full order math model, the fourth-order ROM and second-order ROM. The comparison results are shown in table II. All simulations are conducted with ode4 solver. Fundamental sample time is set as 10μs and the simulation stop time is set as 5s. Mentioned that the simulation time is obtained from the average value of multiple repeated simulations.

TABLE II. SIMULATION SPEED COMPARISON OF DIFFERENT MODELS

Models	Simulation time
Electromechanical model	25s -27s
Full-order math model	5s
The fourth-order ROM	4s
The second-order ROM	2s

It is found that the electromechanical model requires more than five times the simulation time compared to the other models. Among the full-order model and different ROMs, the full-order model requires 1.25 times the simulation time compared to the fourth-order model and 2.5 times the simulation time compared to the second-order model. Therefore, it is necessary to make a trade-off between the accuracy and computational burden.

979-8-3315-8138-1

IV. ACCURACY ANALYSIS OF REDUCED ORDER MODEL

In this sub-section, the accuracy of different ROMs is quantified. The core idea is to analyze the model order reduction error between full-order model, fourth-order ROM and second-order ROM.

First, between the full-order model and fourth-order model, the impact of VCC determines the model order reduction error. The key state variables involved are I_{gd} and I_{gq}. Considering that the I_{gd}, I_{gq} are composed of their reduced order component (ROC) and the model error component (MEC). Define the I_{gd}, I_{gq}'s ROC and MEC as I_{gd_r}, I_{gq_r} and I_{gd_e}, I_{gq_e}, respectively. According to the algebraic constraint of VCC, there is:

$$\begin{cases} I_{gd\_r} = I_{dref} \\ I_{gq\_r} = I_{qref} \end{cases} \tag{13}$$

Substitute $I_{gd} = I_{gd\_r} + I_{gd\_e}$ and $I_{gq} = I_{gq\_r} + I_{gq\_e}$ to the dynamic equation of VCC (5) and the dynamic equation of L_f (7), there is:

$$\begin{cases} \dfrac{dI_{gd\_e}}{dt} = -\dfrac{K_{pc}}{L_f} I_{gd\_e} - \dfrac{K_{pc}}{L_f}\displaystyle\int I_{gd\_e}dt - \dfrac{dI_{gdref}}{dt} \\ \dfrac{dI_{gq\_e}}{dt} = -\dfrac{K_{pc}}{L_f} I_{gq\_e} - \dfrac{K_{pc}}{L_f}\displaystyle\int I_{gq\_e}dt - \dfrac{dI_{gqref}}{dt} \end{cases} \tag{14}$$

Formula (14) is the dynamic equation governing the I_{gd_e} and I_{gq_e}. The input variables are $-dI_{gdref}/dt$ and $-dI_{gqref}/dt$, which is the differential of I_{gd_r}, I_{gq_r} with respect to time. In other words, the MEC of I_{gd}, I_{gq} are determined by both the VCC's parameters and the ROC of I_{gd}, I_{gq}. Figure 6 shows the schematic diagram of the model reduction error of VCC.

Then, between the fourth-order ROM and the second-order ROM, the impact VAC's dynamic determines the model order reduction error. The key state variables involved are I_{dref} and I_{qref}. Similarly, define the ROC and MEC of I_{dref} and I_{qref} as I_{dref_r}, I_{qref_r} and I_{dref_e}, I_{qref_e}, respectively. The I_{gdref_r}, I_{gqref_r} satisfy the algebraic constraint of VAC:

$$\begin{cases} I_{dref\_r} = \dfrac{R_V\left(E_{GFM} - V_g\cos\delta\right) + \omega_n L_V V_g \sin\delta}{\left(R_V\right)^2 + \left(\omega_n L_V\right)^2} \\ I_{qref\_r} = \dfrac{-\omega_n L_V\left(E_{GFM} - V_g\cos\delta\right) + R_V V_g \sin\delta}{\left(R_V\right)^2 + \left(\omega_n L_V\right)^2} \end{cases} \tag{15}$$

Substitute $I_{dref} = I_{dref\_r} + I_{dref\_e}$ and $I_{qref} = I_{qref\_r} + I_{qref\_e}$ to the dynamic equation of VAC (3), the dynamic equation governing the I_{dref_e}, I_{qref_e} is obtained:

$$\begin{cases} \dfrac{dI_{dref\_e}}{dt} = \omega_n I_{qref\_e} - \dfrac{R_V}{L_V} I_{dref\_e} - \dfrac{dI_{dref\_r}}{dt} \\ \dfrac{dI_{qref\_e}}{dt} = -\omega_n I_{dref\_e} - \dfrac{R_V}{L_V} I_{qref\_e} - \dfrac{dI_{qref\_r}}{dt} \end{cases} \tag{16}$$

Similarly, the MEC of I_{dref} and I_{qref} are determined by both the control parameters of VAC and the ROC of I_{dref}, I_{qref}. Figure 7 shows the schematic diagram of the model reduction error of the VAC.

Figure 8 shows the simulation verification of the model order reduction error. The real-time model order reduction error are the solid yellow curves. The calculated MEC of VCC and VAC and I_{gq} are the dashed orange curves. It is obvious that the simulation results are highly consistent with the calculated model order reduction errors, verifying the high accuracy of derived MEC.

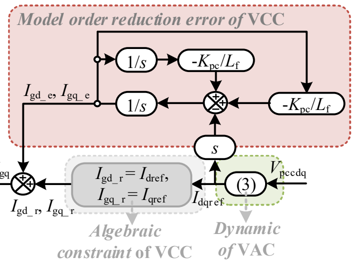

Fig. 6. Schematic diagram of the model reduction error of VCC.

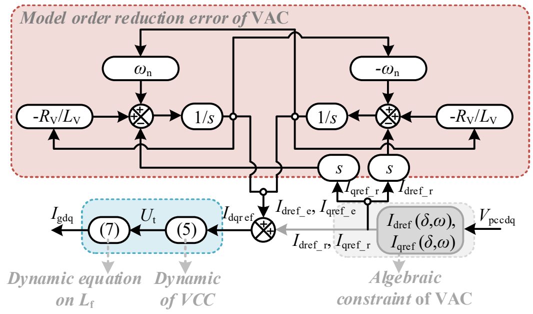

Fig. 7. Schematic diagram of the model reduction error of VAC.

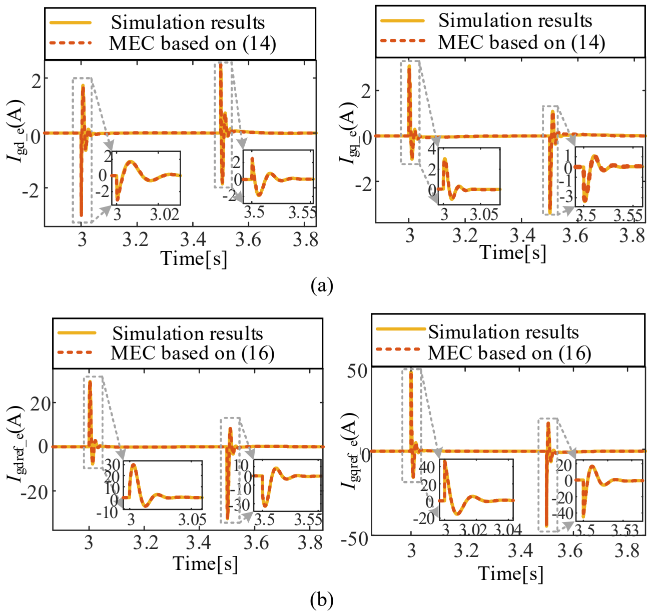

Fig. 8. Simulation verification of the derived MEC. (a) MEC of VCC; (b) MEC of VAC.

Furthermore, according to the dynamic equation shown in (14) and (16), the key parameters that impact the MEC can be obtained. For VCC, the eigenvalues of the state matrix are shown in (17), under the condition that the $K_{pc}^2 - 4K_{ic}L_f > 0$. Since $\lambda_1 > \lambda_2$, the MEC is determined mainly by λ_1. According to the monotonicity analysis of λ_1, it is known that the MEC of VCC is increasing with K_{pc} but decreasing with K_{ic}. Figure 9(a) and (b) show the impact of K_{pc} and K_{ic} on I_{gd_e} and I_{gq_e}. Simulation results are highly consistent with the above theoretical analysis.

$$\begin{cases} \lambda_1 = \dfrac{-K_{pc}/L_f + \sqrt{\left(K_{pc}/L_f\right)^2 - 4K_{ic}/L_f}}{2} \\ \lambda_2 = \dfrac{-K_{pc}/L_f - \sqrt{\left(K_{pc}/L_f\right)^2 - 4K_{ic}/L_f}}{2} \end{cases} \tag{17}$$

For VAC, the eigenvalues of the state matrix are shown in (18), based on the dynamic equation (16). Obviously, R_V/L_V is the key parameter that impacts the MEC of VAC. When R_V/L_V increases, the MEC of VAC will be decreased. On the contrary, the MEC of VAC will be increased. Figure 9(c) shows the impact of R_V/L_V on I_{dref_e} and I_{qref_e}. Simulation results are highly consistent with the above theoretical analysis.

$$\begin{cases} \lambda_1 = \left(-R_V/L_V\right) + j\omega_n \\ \lambda_1 = \left(-R_V/L_V\right) - j\omega_n \end{cases} \tag{18}$$

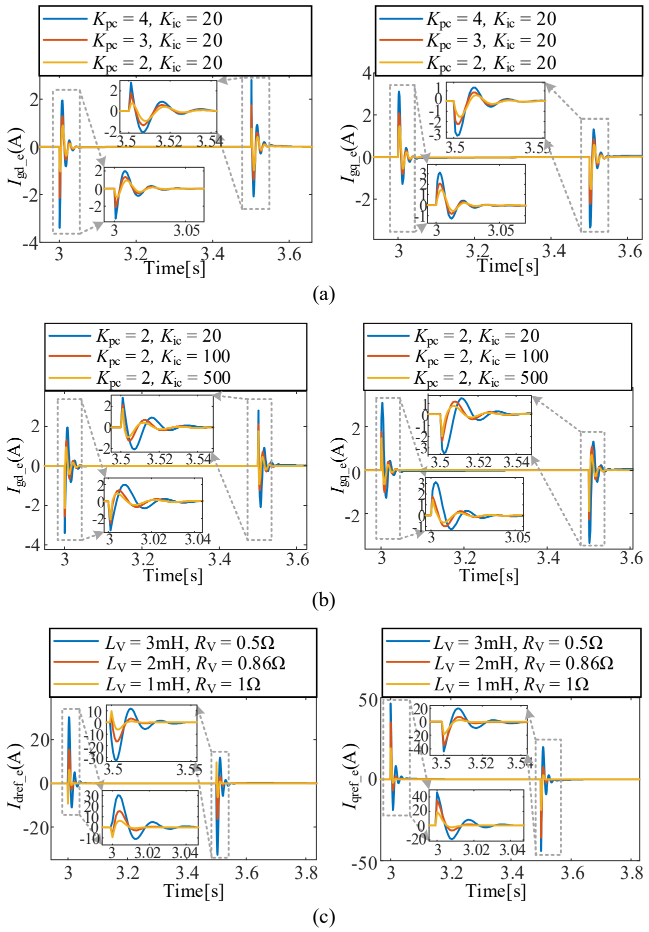

Fig. 9. Impact of parameters' variation on the derived MEC. (a) Impact of R_V/L_V on the MEC of VAC; (b) Impact of K_{pc} on the MEC of VCC; (c) Impact of K_{ic} on the MEC of VCC.

In practical engineering, the MEC of I_{gd} and I_{gq} are not directly adopted as evaluation index of the model applicability. In the power system, the frequency and voltage are the main variables concerned. Therefore, the derived MEC of I_{gd} and I_{gq} need be converted to the MEC of frequency and voltage. Then, the model applicability is assessed based on the frequency and voltage. According to the power system standard [8], the frequency regulation dead band is ±0.02 - ±0.06Hz and the voltage measurement error must not exceed 1% of the rated value. Therefore, when the MEC of frequency and voltage satisfies above standard, the model is applicable.

The MEC of voltage is determined by the dynamic of line inductor L_g (6). Then, the MEC of active power can be calculated based on the MEC of voltage and current. Furthermore, since the frequency is generated by the dynamic of DC-link bus capacitor and matching control, the MEC of frequency can be calculated based on the MEC of active power. Due to the length of paper, detailed derivation process of the frequency and voltage MEC are not provided here. In the future work, the model applicability will be further detailly discussed.

V. Conclusions

In this paper, based on the singular perturbation theory, the reduced order model of matching control GFM-VSC are established. By comparing the simulation speed and accuracy, it is known that a trade-off needs to be made between model accuracy and simulation speed. Then, the model error components between reduced order model and full-order model are quantitatively estimated. It is concluded that the R_V/L_V is the key parameter that impact the model error component of virtual admittance control. The model reduction error of virtual admittance control is decreasing with R_V/L_V. For the vector current control, the proportional gain K_{pc} and integral gain K_{ic} of impact its model reduction error. With $K_{pc}^2 - 4K_{ic}L_f > 0$, the model reduction error of vector current control is increasing with K_{pc} and decreasing with K_{ic}. Accuracy of the derived model reduction error and the impact of parameters' variation are verified through simulation. At last, the model applicability is briefly discussed. In the future work, the applicability of different reduced order models in practical engineering will be further detailly analyzed.

VI. References

[1] S. Curi, D. Groß and F. Dörfler, "Control of low-inertia power grids: A model reduction approach," *IEEE Annu. Conf. Decis. Control, CDC*, Australia, 2017, pp. 5708-5713.

[2] Z. Ma, Z. Wang, Y. Yuan and T. Hong, "Singular Perturbation-Based Large-Signal Order Reduction of Microgrids for Stability and Accuracy Synthesis With Control," *IEEE Trans. Smart Grid*, vol. 15, no. 4, pp. 3361-3374, July 2024.

[3] Y. Ma, D. Zhu, Z. Zhang, X. Zou, J. Hu and Y. Kang, "Modeling and Transient Stability Analysis for Type-3 Wind Turbines Using Singular Perturbation and Lyapunov Methods," *IEEE Trans. Ind. Electron.*, vol. 70, no. 8, pp. 8075-8086, Aug. 2023.

[4] A. Nayak, M. M. Rayguru, S. Mishra and M. J. Hossain, "A Quantitative Approach for Convergence Analysis of a Singularly Perturbed Inverter-Based Microgrid," *IEEE Trans. Energy Convers.*, vol. 36, no. 4, pp. 3016-3030, Dec. 2021.

[5] M. Kabalan, P. Singh and D. Niebur, "Nonlinear Lyapunov Stability Analysis of Seven Models of a DC/AC Droop Controlled Inverter Connected to an Infinite Bus," *IEEE Trans. Smart Grid*, vol. 10, no. 1, pp. 772-781, Jan. 2019.

[6] X. Xiong, C. Wu and F. Blaabjerg, "An Improved Synchronization Stability Method of Virtual Synchronous Generators Based on Frequency Feedforward on Reactive Power Control Loop," *IEEE Trans. Power Electron.*, vol. 36, no. 8, pp. 9136-9148, Aug. 2021.

[7] X. Fu et al., "Large-Signal Stability of Grid-Forming and Grid-Following Controls in Voltage Source Converter: A Comparative Study," *IEEE Trans. Power Electron.*, vol. 36, no. 7, pp. 7832-7840, July 2021.

[8] *Technical requirements for connecting photovoltaic power station to power system,* standard GB/T 19964-2024, Mar. 2024.